Journal of Biomedical Optics

BiomedicalOptics.SPIEDigitalLibrary.org

Europium-quantum dot nanobioconjugates as luminescent probes for time-gated biosensing

Piotr J. Cywiński
Tommy Hammann
Dominik Hühn
Wolfgang J. Parak
Niko Hildebrandt
Hans-Gerd Löhmannsröben

SPIE.

Europium-quantum dot nanobioconjugates as luminescent probes for time-gated biosensing

Piotr J. Cywiński,[a,b,*] Tommy Hammann,[a,b] Dominik Hühn,[c] Wolfgang J. Parak,[c] Niko Hildebrandt,[d] and Hans-Gerd Löhmannsröben[a]
[a]University of Potsdam, Institute of Chemistry, Physical Chemistry, Karl-Liebknecht-Str. 24-25, Potsdam-Golm 14476, Germany
[b]Fraunhofer Institute for Applied Polymer Research, NanoPolyPhotonics, Geiselbergstr. 69, Potsdam-Golm 14476, Germany
[c]Philipp University of Marburg, Faculty of Physics, Biophotonics, Renthof 7, Marburg 35037, Germany
[d]University of Paris-South, Institute for Fundamental Electronics, NanoBioPhotonics, 15 Rue Georges Clémenceau, Orsay 91405, France

Abstract. Nanobioconjugates have been synthesized using cadmium selenide quantum dots (QDs), europium complexes (EuCs), and biotin. In those conjugates, long-lived photoluminescence (PL) is provided by the europium complexes, which efficiently transfer energy via Förster resonance energy transfer (FRET) to the QDs in close spatial proximity. As a result, the conjugates have a PL emission spectrum characteristic for QDs combined with the long PL decay time characteristic for EuCs. The nanobioconjugates synthesis strategy and photophysical properties are described as well as their performance in a time-resolved streptavidin-biotin PL assay. In order to prepare the QD-EuC-biotin conjugates, first an amphiphilic polymer has been functionalized with the EuC and biotin. Then, the polymer has been brought onto the surface of the QDs (either QD655 or QD705) to provide functionality and to make the QDs water dispersible. Due to a short distance between EuC and QD, an efficient FRET can be observed. Additionally, the QD-EuC-biotin conjugates' functionality has been demonstrated in a PL assay yielding good signal discrimination, both from autofluorescence and directly excited QDs. These newly designed QD-EuC-biotin conjugates expand the class of highly sensitive tools for bioanalytical optical detection methods for diagnostic and imaging applications. [DOI: 10.1117/1.JBO.19.10.101506]

Keywords: quantum dots; europium complex; amphiphilic polymer assembly; nanobioconjugate; biosensor; time-resolved fluorescence.

Paper 140119SSRR received Feb. 28, 2014; revised manuscript received Jun. 3, 2014; accepted for publication Jun. 4, 2014; published online Jul. 2, 2014.

1 Introduction

Quantum dots (QDs) are luminescent semiconductor nanocrystals that, due to the quantum confinement effect and macromolecular size, combine unique photophysical features such as broad strong absorption and size-dependent efficient photoluminescence (PL).[1,2] The mobility in liquid phases and high surface-to-volume ratio as well as effective methods established for their bioconjugation make QDs promising objects for bioanalytical techniques including *in vitro* diagnostics and PL imaging.[3] Noticeably, QDs have a reduced tendency for PL self-quenching and photobleaching, which are common drawbacks observed for organic dyes or fluorescent proteins.[4] This improved resistance against photodegradation effects also enables high sensitivity and usability in high-throughput molecular diagnostics.[5] Over the last two decades, QDs have attracted considerable attention as universal luminescent nano-objects for numerous fields including medicine,[6] pharmacology,[7] and chemical sensing.[8] In recent years, various QDs have been used in biological and biomedical applications, such as multiplexed systems for DNA detection,[9] biomarker sensing,[10,11] luminescent immunoassays,[12,13] bioassays,[14] optical coding,[15,16] protein concentration determination,[17] drug tracking,[18] single molecule tracking,[19] photodynamic therapy,[20] and intracellular imaging.[21,22] Continuously, various new QD-based nanosystems are appearing, and new application fields are growing dynamically.

In recent years, numerous systems have been presented in which QDs are combined with organic fluorescent moieties to achieve additional properties beyond those provided solely by QDs. In this direction, a wide variety of systems can be found, including a combination of nanorods and dyes,[23] pyrene-functionalized nanoparticles to detect nitroaromatic compounds such as nitroanilines and nitrobenzenes,[24] CdSe QDs functionalized with a naphthalimide dye to yield unconventional QD quenching,[25] graphene QDs combined with europium ions to recognize phosphates,[26] QD-carbon nanotube conjugates for photoacoustic and PL detection of circulating cells with flow cytometry *in vivo*,[27] doxorubicin-QD conjugates for photo-controlled drug delivery,[28] and QD-europium ion conjugates to detect nucleoside triphosphates.[29] A QD-Lucigenin conjugate sensor has also been developed to sense chloride anions in an aqueous environment with a sensitivity down to around 300 nM.[30] Interesting examples of luminescent QD-based conjugates presented a cascade FRET from a conjugated polymer to a QD and then to an organic dye,[31] or multistep FRET from a Tb-complex to a QD and then to an organic dye.[10,32,33] Very recently, CdTe QDs functionalized with a naphthyridine dye were developed to detect guanosine nucleotides in an aqueous environment.[34] Due to specific and selective naphthyridine-nucleotide interactions combined with the optical properties of the QDs, those conjugates showed improved sensitivity in comparison to naphthyridine or polystyrene

*Address all correspondence to: Piotr Cywiński, E-mail: piotr.cywinski@iap.fraunhofer.de

0091-3286/2014/$25.00 © 2014 SPIE

nanoparticle-based sensors.[35] These nanosensors were able to detect cyclic 3'5' guanosine monophosphate (cGMP) down to 70 ng/mL.

In numerous instances of the above summarized QD-dye systems, Förster resonance energy transfer (FRET) was the main mechanism responsible for the specific signal modulation. FRET is a nonradiative energy transfer from one emitting moiety (donor) to another energy-receiving moiety (acceptor). In fundamental considerations, FRET is a dipole-dipole interaction and it requires both close donor-acceptor spatial proximity (ca. 1 to 20 nm) and spectral overlap between donor emission and acceptor absorption.[36] Lanthanide complexes as FRET donors provide many advantages, which are mainly related to their long excited-state decay times, large effective Stokes' shifts, and well-defined and narrow emission peaks.[37,38] The use of lanthanide complexes in FRET applications facilitates the transfer of their long PL decay times to acceptors, which leads to long-living species emitting at wavelengths different from those of the lanthanide ion. Such systems have been demonstrated with simultaneous FRET to five different acceptors using organic dyes[39] or QDs.[40] Because QDs have very narrow emission bands and large absorption cross sections over a broad wavelength range, they are superior FRET acceptors in combination with lanthanides.[41–43] The lanthanide-to-QD FRET was demonstrated for the first time with biotin-streptavidin-based binding systems using Eu- and Tb-based complexes.[44,45] Although there exist FRET systems that combine lanthanides and QDs, they have always been based on FRET that was enabled by biological recognition (e.g., biotin-streptavidin). A direct integration of lanthanides and QDs within one nanoparticle could overcome the necessity of binding-established FRET and yield a single lanthanide-QD emitter. Apart from medical applications, such QD-based nanoconjugates could find their application in display technologies, where long-living emissions at freely selected and well-defined wavelengths are highly desirable properties.

In this contribution, we present a QD-based conjugate architecture which combines an emission spectrum typical of a QD with a decay time typical of a europium complex. The preparation strategy, photophysical characterization, and the performance in biotin-streptavidin PL assays are also described. The QD-EuC-biotin conjugates have a high potential to be applied to, but not limited to, routine applications in fluoroimmunoassays and cellular imaging.

2 Materials and Methods

2.1 *Materials*

Hydrophobically capped QDs in decane, Qdot® 655 ITK (QD655), Qdot® 705 ITK (QD705), and biotinylated water-dispersible Qdot® 655 (QD655-biotin) were purchased from Life Technologies GmbH (Darmstadt, Germany). Sodium [4'-(4'-Amino-4-biphenylyl)-2,2':6',2''-terpyridine-6,6''-diylbis (methyliminodiacetato)]europate(III) (EuC) was purchased from TCI Deutschland GmbH (Eschborn, Germany). Amine-PEG_3-Biotin and 1 M Sodium Borate Buffer (SBB12) were purchased from Thermo Fisher Scientific GmbH (Ulm, Germany). Cy5-biotin was purchased from Interchim (Montluçon, France). Poly(isobutylene-*alt*-maleic anhydride) (PMA, molecular weight $M_w \approx$ 6 kDa), Dodecylamine (DAM), Triethylamine (NEt_3), and 4-Dimethylaminopyridine (DMAP) were purchased from Sigma Aldrich (Taufkirchen bei München, Germany). Streptavidin was purchased from Promega GmbH (Mannheim, Germany). Biotin-free bovine serum albumin (BSA) was purchased from Carl Roth GmbH + Co. KG (Karlsruhe, Germany). Double distilled water (conductance $G = 0.055\ \mu$S), used during PL assay experiments, was prepared using an Arium® Comfort water purification system (Sartorius AG, Göttingen, Germany). All chemicals were used without further purification.

2.2 *Methods*

2.2.1 *Preparation of quantum-europium complex-biotin nanoconjugates*

Preparation of the PMA-europium-biotin. The QD655/705-EuC conjugates have been prepared according to the following general protocol. The PMA preparation procedure has been described in detail elsewhere.[46] Briefly, 1 eq. (related to the number of monomer units) of PMA, 0.75 eq. of DAM, 0.77 eq. of NEt_3, 0.1 eq of DMAP, 0.02 eq. of EuC, and 0.02 eq. of PEG-biotin were dissolved in THF and stirred under reflux for 24 h (80°C). NEt_3 and DMAP serve as nucleophilic compounds, which promote the opening of maleic acid anhydride rings and thus the formation of an amide bond. This formation occurs because the opened rings provide two carboxylic groups each, which can react with the primary amines of DAM, EuC, or PEG-biotin. By this procedure, 75% of monomer units were reacted with DAM (hydrophobic side chains), 2% with EuC, and 2% with PEG-biotin. The rest of the anhydride rings was believed to remain unreacted. Thus, a total 22.8% of unreacted monomer units and one carboxylic group per reacted/opened ring were available for further functionalization or could serve for the later colloidal stabilization of QDs. After the conjugation reaction, the solvent was evaporated to dryness and the remaining solid was redissolved in chloroform to a 50 mM solution (related to the number of PMA monomer units).

Quantum dot coating with PMA-europium-biotin. The QDs, originally delivered in decane, were transferred into chloroform according to the flocculation protocol provided by the manufacturer (precipitation with the fourfold volume of a 75/25 methanol/isopropanol mixture *via* centrifugation and redissolution in chloroform). Then, the QDs were mixed with PMA-EuC-biotin solution also in chloroform.[46] The amount of added polymer was chosen in a way to assure a defined number $R_{P/\mathrm{Area}}$ of the monomers per nm^2 of the effective QD surface.[46] The effective QD surface refers to the effective diameter d_{eff}, which is composed of the semiconductor core/shell diameter d_c and the thickness of the surface capping d_p ($d_{\mathrm{eff}} = d_c + 2 \cdot d_p$).

The core diameter d_c, employed in the coating procedure, is calculated in a way that d_c corresponds to a sphere with an equivalent surface area A compared to a rod with length $d_{c,1}$ and width $d_{c,2}$. Thus, d_c was determined as follows:

$$A_{\mathrm{sphere}} = A_{\mathrm{rod}}. \tag{1}$$

$$\pi d_c^2 = \pi d_{c,2}\left(d_{c,1} + \frac{d_{c,2}}{2}\right). \tag{2}$$

$$d_c = d_{c,2} \cdot \sqrt{\frac{d_{c,1}}{d_{c,2}} + \frac{1}{2}}. \tag{3}$$

In this manner, the core diameters of QD655 and QD705 were determined to be $d_c = (9.6 \pm 0.6)$ and $d_c = (9.4 \pm 0.7)$ nm. The larger PL emission wavelength of the QD705 despite the smaller size is caused by the different core/shell material. QD655 is CdSe/ZnS, whereas QD705 is CdSeTe/ZnS. This material difference is also the reason for the much broader PL emission spectrum of QD705 compared to QD655. As the QD shape is elongated, d_c refers to the diameter of a spherical QD that would lead to the same surface area like a rod with length $d_{c,1}$ and width $d_{c,2}$. Regarding the employed amount of polymer for QD655 or QD705, $R_{P/\mathrm{Area}}$ was 125 or 130 nm^{-2}, respectively. The mixture was heated to 45°C for 10–15 min and the solvent was then subsequently evaporated under reduced pressure. Then, the solid was redissolved in approximately 1 mL chloroform. This heating-evaporating procedure was repeated three times. Afterward, the dry QDs were dissolved in 50 mM sodium borate buffer, pH = 12 (SBB12). Then, a syringe filter (0.22 μm, Carl Roth, P818.1) was used to remove QD agglomerates and residual cross-linked polymer aggregates. The filtrated solution was concentrated with 100 kDa centrifugation filters (Sartorius, VS2042) and purified via gel electrophoresis in 2% agarose/0.5 × tris borate EDTA (TBE) buffer (pH ≈ 8.0) to remove remaining empty polymer micelles and unreacted reagents.[46,47] Further purification was done in double distilled water with 100 kDa centrifugation filters (five times). The sample concentration has been determined from absorption measurements. As provided by the supplier, the extinction coefficient values at the first exciton peak equal to $0.9 \cdot 10^6$ $\mathrm{M}^{-1}\,\mathrm{cm}^{-1}$ for QD 655 and $0.5 \cdot 10^6$ $\mathrm{M}^{-1}\,\mathrm{cm}^{-1}$ for QD705 were taken for the concentration determination.

2.2.2 *Photoluminescence measurements*

Steady-state PL emission and excitation spectra were recorded using a FluoroMax 4 (Horiba, Jobin Yvon GmbH, Unterhaching, Germany) spectrophotometer working with a continuous 450 W Xe lamp. The samples were excited at 337 nm to provide the same excitation conditions as for time-resolved spectroscopy. The spectra were collected at 2 nm bandpass and an integration time equal to 0.5 s. Additionally, a 390 nm cut-off longpass filter was used to eliminate second-order effects. All spectra were corrected for the instrumental response. In this experiment, 100 μl of 50 nM nanobioconjugate solutions were measured in microcuvettes (130 μl) from Hellma Analytics GmbH (Jena, Germany).

The time-resolved PL measurements were carried out on a Nanoscan PL multifunctional immunoassay reader (IOF Innovative Optische Messtechnik GmbH, Berlin, Germany). A nitrogen laser ($\lambda_{ex} = 337$ nm, repetition rate 20 Hz) was used as an excitation source. The PL signals were collected in a 6 ms (for QD-EuC-biot) and 200 ns (for QD-biot) time window using two photomultipliers with bandpass filters around the emission spectrum of the donor [(620 ± 10) nm] and around the emission spectrum of the acceptor [(665 ± 13) nm for the QD655 and (740 ± 13)nm for the QD705] channel. Filters in the acceptor channel were selected to minimize spectral crosstalk of the donor (EuC) emission into the acceptor channel. The PL of the QDs and the EuC was also measured separately to estimate the background signal. In this experiment, 100 μl of 50nM nanobioconjugate solutions were measured in wells of a nonbinding microtiter plate.

2.2.3 *Photoluminescence bioassays using quantum dot-europium complex-biotin*

1, 2, and 3 μg/mL (19, 38 and 57 nM) streptavidin solutions in phosphate-buffered saline (PBS) were incubated overnight at 4° C in selected wells of a microtiter plate (high-binding Lumitrac 600 plate). The incubation leads to adsorption of streptavidins on the well bottom. A well filled only with PBS was used to provide a reference zero value. For each streptavidin concentration three wells were filled. Then, the streptavidin solution was removed and the wells were washed manually with PBS. Next, in order to reduce a nonspecific interaction between QD-EuC-biotin and the plate surface, the wells were blocked for 1 h with 2% BSA solution in PBS. Then, the BSA solution was removed and the wells were washed manually with PBS and 50 μL of 50 nM QD-EuC-biotin conjugates solution in PBS were added to the streptavidin-modified wells and incubated for 1 h at room temperature. Then, the nanoconjugate solution was removed and the wells were washed three times with PBS. After a final washing step, the wells were filled with 150 μL PBS and the PL decays signals were collected. The decays were integrated over a 200–2000 μs timeframe (time-gated intensity measurement) to receive the final values presented in Fig. 5. Control experiments with QD655-biotin were executed in the same manner. However, the decays were integrated over a 20–200 ns timeframe. The biotin-Cy5 conjugate was used to validate streptavidin coating throughout all experiments.

3 Results and Discussions

Hydrophobically capped QDs were transferred into aqueous solution using overcoating with an amphiphilic polymer, which has advantages and disadvantages compared to standard ligand–exchange protocols.[22,48,49] Depending on the method, several properties can be varied: the distance between attached ligands and the QD surface, nonspecific ligand-QD surface interaction, and colloidal stability.[48,49] Prior to the practical applications, this consideration should be taken into account and the method to transfer initially hydrophobic QDs into aqueous solution needs to be selected based upon the particular requirements of the application. In our present case, we desired QDs with a high colloidal stability and thus opted for coating them with an amphiphilic polymer.[46]

The polymer prepared within this study and its arrangement on a QD is shown in Fig. 1. The octyl chains of trioctylphosphine oxide (TOPO), which are present on the hydrophobic QDs as supplied by the vendor, intercalate in organic solvent with the dodecyl chains of the amphiphilic polymer (by hydrophobic interaction) to form a hydrophobic buffering shell around the QD.[46] Importantly, the amphiphilic polymer backbone is built of maleic anhydride rings. When placed in aqueous solution, the maleic anhydrides hydrolyze, which results in a large number of carboxylic moieties on the QD surface to provide the QDs with colloidal stability.

The maleic anhydride rings also facilitate uncomplicated coupling of amine-containing molecules to the polymer through amide bond formation, which in the present cases has been used to premodify the polymer (before coating the QDs) with EuC-PEG-biotin.[46] After transfer of the polymer-coated QDs to an aqueous solution, the carboxylic moieties would also facilitate an uncomplicated polymer postfunctionalization in an aqueous environment, e.g., *via* 1-ethyl-3-(3-dimethylaminopropyl) carbodiimide (EDC) coupling. As seen in Fig. 2, after the

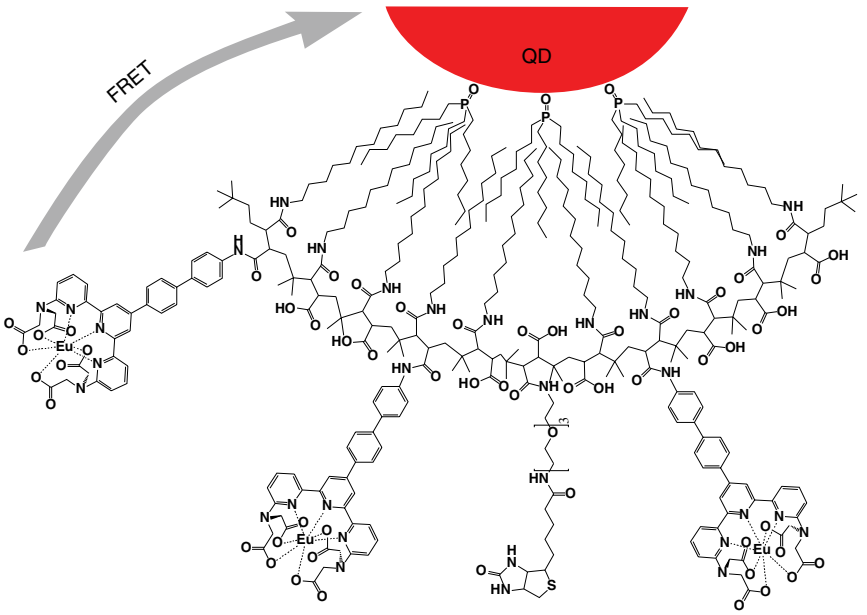

Fig. 1 The assembly of the functional polymer on the QD surface. The QD (either QD655 or QD705) is surrounded by trioctylphosphine oxide chains (coming from the QD preparation) assembled with the dodecyl chains of the amphiphilic polymer. Biotin (to facilitate binding to streptavidin) and EuC (to pump QD with long-living emission) were incorporated into the polymer prior to its assembly on the QD. The remaining carboxylic moieties facilitate stability and solubility of such construct in aqueous solutions.

preparation process, the EuC-polymer emission spectra remained in good agreement with the spectra typical for EuC. Only the relative emission intensities have changed reflecting the change in the immediate vicinity of the complex. Additionally, the EuC-polymer excitation spectrum was shifted about 15 nm to the red.

In our system, efficient FRET is observed due to close spatial proximity between EuC donors in the polymer shell and the QD acceptors. A distance estimation based on assuming a separation of the EuC from the inorganic QD surface by ~30 single C-C bonds (each with a length of 0.12–0.15 nm) yields a distance of 3–5 nm, assuming the dodecyl chains in their extended form. For calculation of FRET efficiencies, one also needs to take into account the distance from the QDs surface to its center corresponding to the dipole center. Using the core/shell radius $r_c(=d_c/2)$, which is around $r_c = 3$–5 nm for both kinds of QDs, the estimated EuC-QD donor–acceptor distance is approximately $r = 6$–10 nm. With a Förster radius of $R_0 = 10$ nm for the EuC-QD655 system,[17] we calculated a FRET-efficiency $[\eta_{\mathrm{FRET}} = (R_0^6)/(r_6 + R_0^6)]$ of $\eta_{\mathrm{FRET}} = 0.5$–$0.96$. Notice that the Förster radius is a theoretical value, which depends on (1) donor quantum yield in the absence of an acceptor, (2) overlap between the donor's emission and the acceptor's absorption, (3) the orientation factor between both dipoles, and (4) the refractive index of the medium.

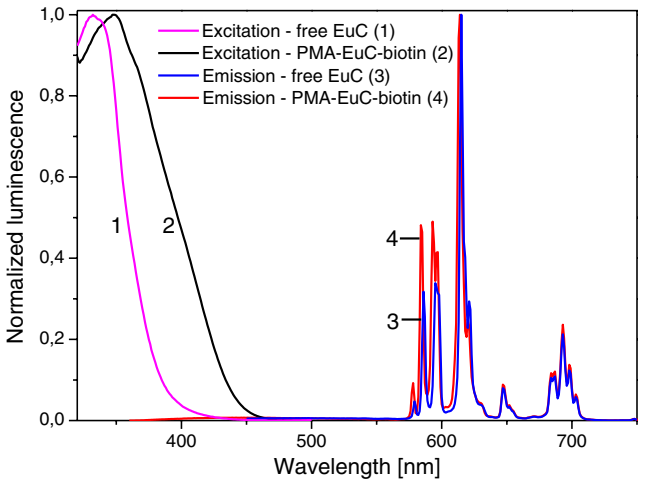

Fig. 2 Steady-state PL excitation and emission spectra taken for EuC free in solution and when conjugated to the amphiphilic polymer.

Time-gated intensity detection in time-resolved spectroscopy allows for minimizing the undesired background effects resulting from directly excited QDs. Under ultraviolet (UV) light excitation at 337 nm, the QDs are excited both directly and indirectly through FRET. In a detection timeframe starting from 100 μs, PL coming from directly excited QDs is negligible and the emission coming from FRET-sensitized QDs can mainly be observed. Regarding the extinction coefficients of EuC [$\varepsilon(\mathrm{EuC}) = 31{,}000\ \mathrm{M}^{-1}\,\mathrm{cm}^{-1}$ [50]] and the QDs [$\varepsilon(\mathrm{QD655}) = 11{,}500{,}000\ \mathrm{M}^{-1}\,\mathrm{cm}^{-1}$ and $\varepsilon(\mathrm{QD705}) = 17{,}000{,}000\ \mathrm{M}^{-1}\,\mathrm{cm}^{-1}$ [at 337 nm, which presents a ca. 350-to-550-fold larger absorptivity for the QDs, the steady-state contribution of EuC to the emission spectra of EuC-QD samples can be neglected and therefore an interpretation of steady-state spectra for EuC-to-QD FRET is not conclusive. For time-resolved measurements, we used a bandpass filter, which passes light at a QD-characteristic (Eu-characteristic) wavelength and blocks most of the contributions from Eu-emission (QD-emission). In our case, the crosstalk of the time-gated EuC emission intensity to the acceptor channel was found to be 5% (at 655 ± 13 nm) and 1% (at 740 ± 13 nm) of the intensity value collected in the donor channel at (620 ± 10) nm.

In Fig. 3, steady-state PL measurements are presented for the QD-EuC nanocomplexes. In those spectra, residual emission in

the 400–500 nm range can be observed, which we attributed to emission of the terpyridine present in the EuC organic antenna. The terpyridine emission is most probably due to an extraction of Eu^{3+} ions from the chelating antenna during purification using gel electrophoresis. This assumption is supported by emission spectra of the EuC-functionalized polymer before coating to the QD (Fig. 2), which did not show any terpyridine emission. In order to "recharge" the antennas with Eu^{3+} ions, we added 10 μL of 25 mM $EuCl_3$ (in 50 mM citric acid, pH = 4) to the 120 μL solution of 50 nM QD-EuC. Adding a large excess of $EuCl_3$ allowed the chelates that have lost their ions to coordinate new Eu^{3+} ions in order to guarantee a maximum chelate recovery for efficient FRET to the QDs. The resulting spectra gave evidence of two main effects. First, the addition of $EuCl_3$ led to a strong reduction in the terpyridine emission, thus indicating the successful Eu^{3+} coordination into the chelating antenna. Compared to the QD655-EuC samples [Fig. 3(a)], the suppression of terpyridine emission becomes much more evident for the QD705-EuC samples [Fig. 3(b)]. This effect can be associated with different amounts of Eu^{3+} ions extracted from the terpyridine chelating antennas for those two systems. In parallel to the decrease of antenna emission, the QDs emission intensity is strongly increased (fivefold for QD655 and threefold for QD705), which suggests that these two processes are related to each other by the improved EuC-to-QD FRET. However, taking into account the large difference in molar absorptivities of EuC and the QDs (vide supra), the strong QD PL intensity increases cannot be purely caused by FRET from EuC to QD. We assume that this effect is a mixture of QD-stabilization (increasing the steady-state PL intensity of directly excited QDs) and increased FRET-sensitization by EuC.

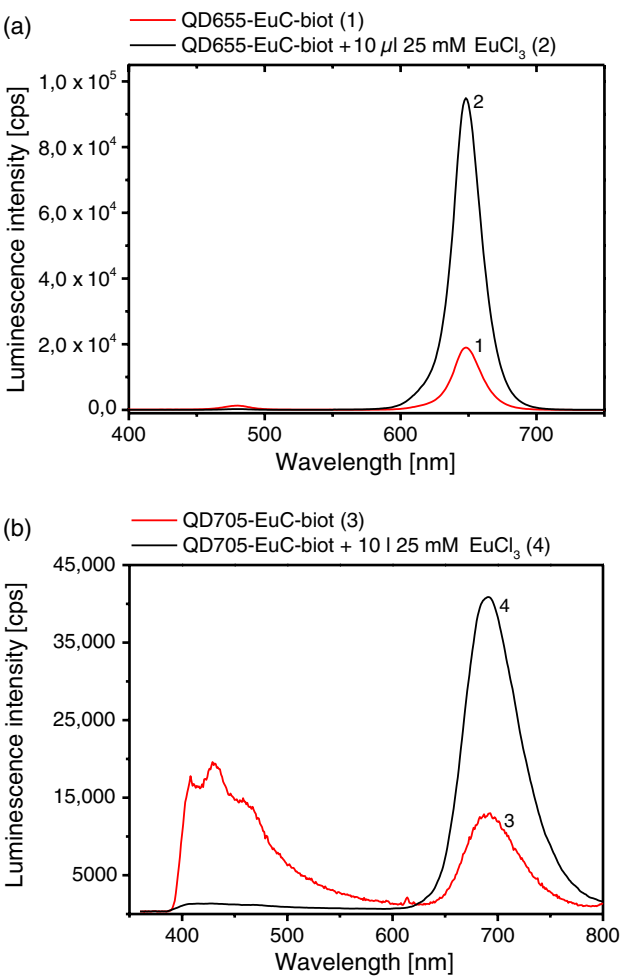

Fig. 3 Luminescence emission spectra (λ_{ex} = 337 nm) of QD655-EuC-biotin (a) and QD705-EuC-biotin (b) nanoconjugates before (blue) and after addition of 10 μL (black) of 25 mM $EuCl_3$ in 50 mM citric acid, pH = 4.

In order to verify that the addition of $EuCl_3$ leads to efficient FRET from EuC to QD (and not only better QD emitters), we performed time-resolved PL measurements. The PL decays for QD655, EuC, and QD655-EuC-biotin are shown in Fig. 4.

Similarly to the steady-state measurements, in time-resolved measurements an increase in QD PL is also observed upon $EuCl_3$ addition to the nanoconjugate solution. However, PL decay curves (taken over a 6 ms timeframe) clearly show QD-FRET sensitization by long-living EuC. The black curve in Fig. 4(a) contains a microsecond decay component which is caused by strong direct excitation of the QDs and the buffer by the nitrogen laser. Although QD decay after direct excitation only lasts several microseconds (decay times with tens to hundreds of nanoseconds), the decay in Fig. 4 lasts up to <1 ms. This decay is caused by saturation of the detection setup directly after intense-pulsed nitrogen laser-excitation [which can even be found for pure PBS buffer excitation, cf. red curve in Fig. 4(b)] and thus mainly reflects the instrumental response. The green curve in Fig. 4(a) contains several decay components:

1. *detector saturation*: short lifetime instruments' response (pure QD and buffer excitation via strong nitrogen–laser pulses), which causes an intensity offset in the first few hundred microseonds;
2. *pure EuC PL*: unquenched long-lifetime EuC PL [weak but significant EuC PL detected in the QD channel at 655 ± 13 nm, cf. Fig. 2 for spectrum and black curve in Fig. 4(b) for decay], which is the main cause for PL detected after ca. 2 ms;
3. *FRET*: long-lifetime QD PL (from EuC-to-QD FRET), which causes an intensity offset up to ca. 2 ms.

Addition of $EuCl_3$ leads to a strong intensity increase of the FRET component, whereas the pure EuC PL and detector saturation components remain unchanged [blue curve in Fig. 4(a)]. The decay curve of pure $EuCl_3$ in solution [green curve in Fig. 4(b)] is only slightly more intense than and has a similar time range to that of the buffer decay [red curve in Fig. 4(b)]. Therefore, the intensity increase from the green to the blue curves in Figure 4(a) cannot be attributed to PL originating from pure Eu^{3+} ions in the sample solution. In order to quantify the single contributions, we fitted the decay curves with a triexponential function Eq. (1), which takes into account detector saturation (τ_1), pure EuC PL (τ_2), and FRET (τ_3).[51]

$$I(t) = a\left[A_1 \exp\left(-\frac{t}{\tau_1}\right) + A_2 \exp\left(-\frac{t}{\tau_1}\right) + A_3 \exp\left(-\frac{t}{\tau_3}\right)\right]. \quad (4)$$

Here A_1, A_2, and A_3 are the amplitude fractions (with $A_1 + A_2 + A_3 = 1$). Because the short decay component is caused by the instrument response to a very strong short-lived signal, this component cannot be taken into account for

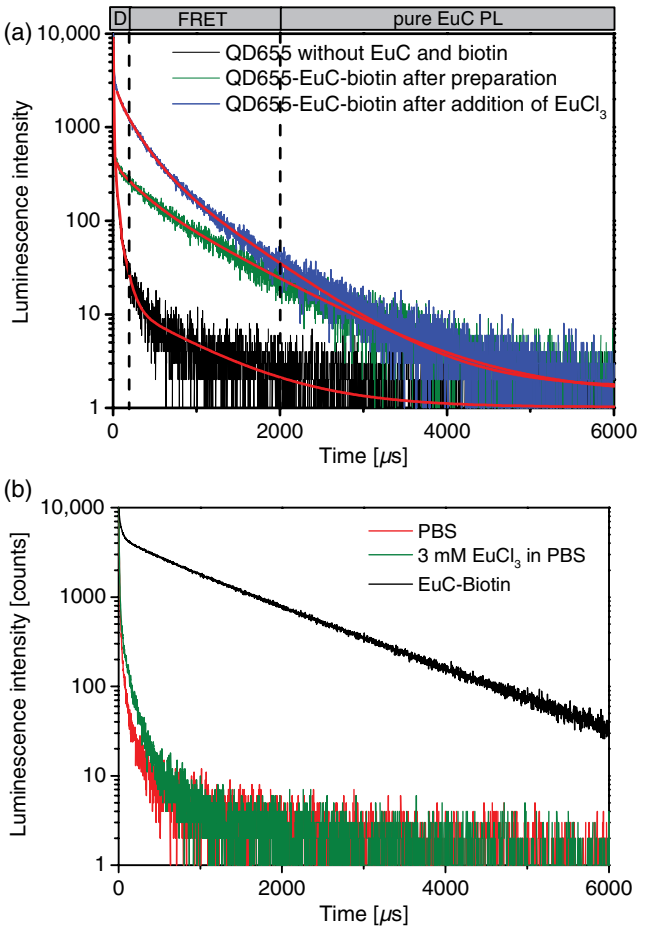

Fig. 4 (a) PL decays collected for QD655 without EuC and biotin (black curve), QD655-Eu-biotin before (green curve) and after (blue curve) the addition of 10 μL of 25 mM $EuCl_3$ in 50 mM citric acid, pH = 4. ($\lambda_{exc} = 337$ nm, emission bandpass filter – (665 ± 13) nm). The red curves correspond to fits with a triexponential function. The different time zones indicated on top of the graph represent the different PL intensity contributions of detector saturation D (instrument response), FRET, and pure (unquenched) EuC PL. (b) Control experiments showing the decays collected for pure PBS buffer (red curve), 3 mM $EuCl_3$ in PBS (green curve), and the EuC-biotin polymer in PBS (black curve). Note: The EuC-biotin decay is shown to illustrate the long decay of pure EuC. As it was collected for a pure EuC polymer solution (without attachment to QD655 and subsequent separation of pure EuC), it had a significantly higher concentration and intensity than the pure EuC PL presented in Fig. 4(a).

a quantitative evaluation of direct QD excitation. The QDs are very strongly excited at 337 nm and therefore emit a very strong PL signal. As mentioned above, this strong signal saturates the photomultiplier detectors; therefore, the observed decay represents a detection setup decay signal of the photomultiplier electronics rather than the optical decay of the QDs. However, fitting for this component allows a subtraction of this unwanted background and a re-evaluation and quantification of the unquenched EuC and the FRET-sensitized QD components using Eq. (2):

$$I(t) = a\left[A_1 \exp\left(-\frac{t}{\tau_1}\right) + b\left\{B_2 \exp\left(-\frac{t}{\tau_2}\right) + B_3 \exp\left(-\frac{t}{\tau_3}\right)\right\}\right], \quad (5)$$

where B_2 and B_3 are the amplitude fractions of unquenched EuC and FRET-sensitized QD, respectively ($B_2 + B_3 = 1$). The decay times summarized in Table 1 were obtained from decays presented in Fig. 4(a) for QD655-EuC-biotin conjugates before and after adding $EuCl_3$ [calculated using Eqs. (1) and (2)]. The decay times determined from decays collected for solutions containing only EuC or QD655 have been added for comparison. PL decays either of QDs or EuC have been fitted with a monoexponential function, assuming the existence of only one species in solution. The decay components of unquenched EuC (B_2 and τ_2) and FRET-sensitized QD (B_3 and τ_3) show almost equal amplitude fractions of unquenched EuC (42%) and FRET-sensitized QDs (58%) for the QD655-EuC samples before addition of $EuCl_3$. After $EuCl_3$ addition, the amplitude fraction determined for unquenched EuC was reduced to 14%, while the one for FRET-sensitized QDs increased to 86%. This behavior corresponds to a significant increase of FRET-quenched EuC and FRET-sensitized QDs and is thus clear evidence for enhanced EuC-to-QD FRET upon addition of $EuCl_3$. At the same time, this enhancement does not correspond to an enhanced FRET efficiency because the FRET decay time (τ_3) does not significantly change. It is rather a sign for more EuC that are available for transferring their energy to a QD.

Based on the average FRET-decay time value ($\langle\tau_3\rangle = 230 \pm 20$ μs) and the average decay time of unquenched EuC ($\langle\tau_2\rangle = 900 \pm 130$ μs), the FRET efficiency was calculated to be $\eta_{FRET} = 1 - \langle\tau_3\rangle/\langle\tau_2\rangle = 0.74 \pm 0.6$. Using the Förster radius of $R_0 = 10$ nm, this leads to an average EuC-QD donor–acceptor distance of $r = R_0[\langle\tau_3\rangle/(\langle\tau_2\rangle - \langle\tau_3\rangle)]^{1/6} = 8.4 \pm 0.5$ nm, which is in very good agreement with the estimated distance range from 6 to 10 nm (vide supra) and with previously determined values for the organic polymeric shell thickness.[47]

3.1 *Photoluminescence Bioassay*

The biotin–streptavidin recognition system is often used in biological recognition assays due to having the highest binding affinity constant (ca. 10^{-14} mol/L) known for noncovalent interactions. Due to the strong biotin-streptavidin interaction, biotin is a convenient chemical group to test the biosensing usability of our complexes in an uncomplicated way. In our

Table 1 The decay times τ_i and corresponding amplitudes A_i and B_i obtained from fitting PL decays in Fig. 4 using Eqs. (1) and (2). QD655-EuC-biotin (1) corresponds to the sample resulting from nanobioconjugate preparation and QD655-EuC-biotin (2) to the sample after addition 10 μL of $EuCl_3$.

	τ_1 [μs]	A_1	τ_2 [μs]	A_2 B_2	τ_3 [μs]	A_3 B_3
QD655-EuC-biotin (1)	26.5	0.47	910	0.22 0.42	238	0.31 0.58
QD655-EuC-biotin (2)	26.9	0.29	770	0.10 0.14	220	0.61 0.86
EuC	–	–	1020	1	–	–
QD655	27.5	1	–	–	–	–
Average decay times	27	–	900	–	230	–

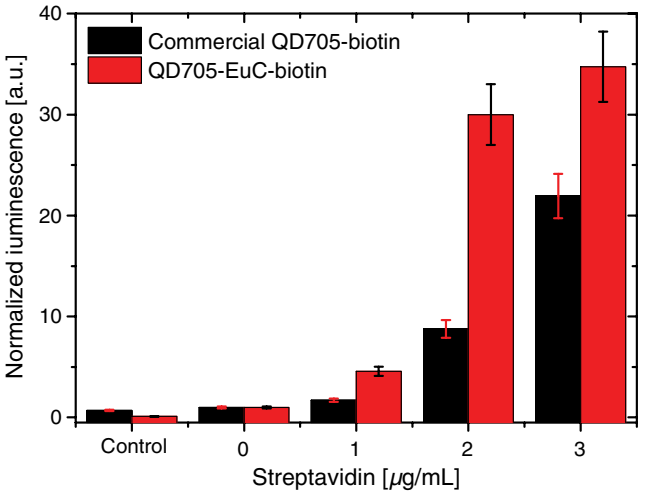

Fig. 5 PL signal (integrated over 1800 μs (200–2000 μs) of QD655-EuC-biotin and commercial biotinylated QD655 [integrated over 180 ns (20–200 ns)] collected in microtiter plate wells covered with 1, 2, and 3 μg/mL of streptavidin. The signals were normalized to 1 corresponding to 0 μg/mL streptavidin. A well only with BSA without streptavidin (0 μg/mL) has been added to test nonspecific interactions. The control corresponds to a signal from a well in which no BSA and no streptavidin was present.

study, the PEG-biotin was attached to the amphiphilic polymer to provide biotin functionality to the QD655-EuC-biotin. Microtiter plate wells covered with different streptavidin concentrations (1, 2, 3 μg/mL) were exposed to 50 nM QD655-EuC-biotin solutions in PBS. After incubation with QD655-EuC-biotin (and QD655-biotin as a control) and subsequent washing, the PL assays were performed using time-gated (200–2000 μs) PL intensity detection (20–200 ns time gate for QD655-biotin). The assay results are presented in Fig. 5. One can observe an enhancement in the PL signal with increasing streptavidin concentration. Notably, for the presented system, we could observe a 30-fold enhancement in PL from 0 to 2 μg/ml (0–38 nM) streptavidin, which is remarkable in comparison to the situation when only QDs are used. We note that the detection setup for the QD655 biotin is not optimal because time gating and UV excitation at low repetition rates would not be necessary. However, in order to be able to use the same experimental conditions, we also used time gating in a relevant time range for QD PL emission. Even without this comparison, our results demonstrate a highly sensitive detection of biotin–streptavidin binding, and therefore, the potential of our nanobioconjugates for their use in PL bioassays such as heterogeneous immunoassays. For example, in a heterogeneous assay (washing after each step is omitted in the following description) a primary "catcher" antibody is adsorbed on the well surface. After passivation, the catcher antibodies are exposed to a sample containing an analyte, i.e., an antigen. Then, a secondary antibody (e.g., conjugated with a fluorescent dye) – a "detector" – is added for quantification. Replacing the fluorescent dye on the detector antibody with streptavidin would allow the attachment of our biotinylated nanobioconjugate and a sensitive time-gated detection without autofluorescence background. Using different QD colors (e.g., QD655 and QD705 as in our study) would allow for multiplexed time-gated detection. Apart from the use in immunoassay, such constructs can find their application in other fields such as imaging or display technologies.

4 Conclusions

In this study, we presented a method to design nanobioconjugates that constitute a new approach for novel QDs with long-lived PL emission. The presented QD-EuC-biotin nanobioconjugates extend the range of materials that can be applied in fluoroimmunoassays, imaging, flow cytometry, or microfluidic optical sensing systems. In such applications, the EuC-QDs can possibly improve the signal-to-noise ratio due to strongly reduced autofluorescence detection when compared to QDs with short PL decay times.

Acknowledgments

This research was supported by the Marie Curie European Reintegration Grant QUANTUMDOTIMPRINT (PERG05-GA-2009-247825), the German Research Foundation (DFG, project PA 794/11-1), and the European Commission (project Namdiatream).

References

1. A. H. Fu et al., "Semiconductor nanocrystals for biological imaging," *Curr. Opin. Neurobiol.* **15**(5), 568–575 (2005).
2. E. Petryayeva, W. R. Algar, and I. L. Medintz, "Quantum dots in bioanalysis: a review of applications across various platforms for fluorescence spectroscopy and imaging," *Appl. Spectrosc.* **67**(3), 215–252 (2013).
3. Z. Jin and N. Hildebrandt, "Semiconductor quantum dots for in vitro diagnostics and cellular imaging," *Trends. Biotechnol.* **30**(7), 394–403 (2012).
4. U. Resch-Genger et al., "Quantum dots versus organic dyes as fluorescent labels," *Nat. Methods* **5**(9), 763–775 (2008).
5. K. K. Jain, "Nanodiagnostics: application of nanotechnology in molecular diagnostics," *Expert Rev. Mol. Diagn.* **3**(2), 153–161 (2003).
6. X. Michalet et al., "Quantum dots for live cells, in vivo imaging, and diagnostics," *Science* **307**(5709), 538–544 (2005).
7. M. Geszke-Moritz and M. Moritz, "Quantum dots as versatile probes in medical sciences: synthesis, modification and properties," *Mater. Sci. Eng. C-Mater. Biol. Appl.* **33**(3), 1008–1021 (2013).
8. J. M. Costa-Fernandez, R. Pereiro, and A. Sanz-Medel, "The use of luminescent quantum dots for optical sensing," *Trac-Trends Anal. Chem.* **25**(3), 207–218 (2006).
9. X. Ai, Q. Ma, and X. Su, "Multiplex DNA sensor for BRAF and BRCA detection," *Anal. Biochem.* **438**(1), 22–28 (2013).
10. W. R. Algar et al., "Multiplexed tracking of protease activity using a single color of quantum dot vector and a time-gated Forster resonance energy transfer relay," *Anal. Chem.* **84**(22), 10136–10146 (2012).
11. R. Freeman et al., "Optical aptasensors for the analysis of the vascular endothelial growth factor (VEGF)," *Anal. Chem.* **84**(14), 6192–6198 (2012).
12. K. D. Wegner et al., "Quantum-dot-based forster resonance energy transfer immunoassay for sensitive clinical diagnostics of low-volume serum samples," *ACS Nano* **7**(8), 7411–7419 (2013).
13. K. D. Wegner et al., "Nanobodies and nanocrystals: highly sensitive quantum dot-based homogeneous FRET-immunoassay for serum-based EGFR detection," *Small* **10**(4), 734–740 (2014).
14. P. J. Cywiński et al., "Photophysical evaluation of a new functional terbium complex in FRET-based time-resolved homogenous fluoroassays," *Phys. Chem. Chem. Phys.* **16**(13), 6060–6067 (2014).
15. L. L. del Mercato et al., "Multiplexed sensing of ions with barcoded polyelectrolyte capsules," *ACS Nano* **5**(12), 9668–9674 (2011).
16. S. Fournier-Bidoz et al., "Facile and rapid one-step mass preparation of quantum-dot barcodes," *Angew. Chem. Int. Ed.* **47**(30), 5577–5581 (2008).
17. H. Härmä et al., "Protein quantification using resonance energy transfer between donor nanoparticles and acceptor quantum dots," *Anal. Chem.* **85**(5), 2921–2926 (2013).

18. K. V. Chakravarthy et al., "Doxorubicin-conjugated quantum dots to target alveolar macrophages and inflammation," *Nanomed.: Nanotechnol. Biol. Med.* **7**(1), 88–96 (2011).
19. S. Clarke et al., "Covalent monofunctionalization of peptide-coated quantum dots for single-molecule assays," *Nano Lett.* **10**(6), 2147–2154 (2010).
20. R. Bakalova et al., "Quantum dot anti-CD conjugates: are they potential photosensitizers or potentiators of classical photosensitizing agents in photodynamic therapy of cancer?," *Nano Lett.* **4**(9), 1567–1573 (2004).
21. J. B. Delehanty, H. Mattoussi, and I. L. Medintz, "Delivering quantum dots into cells: strategies, progress and remaining issues," *Anal. Bioanal. Chem.* **393**(4), 1091–1105 (2009).
22. G. Palui et al., "Photoinduced phase transfer of luminescent quantum dots to polar and aqueous media," *J. Am. Chem. Soc.* **134**(39), 16370–16378 (2012).
23. M. Artemyev, "Resonance energy transfer in conjugates of semiconductor nanocrystals and organic dye molecules," *J. Nanophotonics* **6**(1), 061705 (2012).
24. C. E. Agudelo-Morales, R. E. Galian, and J. Perez-Prieto, "Pyrene-functionalized nanoparticles: two independent sensors, the excimer and the monomer," *Anal. Chem.* **84**(18), 8083–8087 (2012).
25. J. Aguilera-Sigalat et al., "Unconventional fluorescence quenching in naphthalimide-capped CdSe/ZnS nanoparticles," *J. Phys. Chem. C* **117**(14), 7365–7375 (2013).
26. J.-M. Bai et al., "Graphene quantum dots combined with europium ions as photoluminescent probes for phosphate sensing," *Chem.-a Euro. J.* **19**(12), 3822–3826 (2013).
27. D. A. Nedosekin et al., "Synergy of photoacoustic and fluorescence flow cytometry of circulating cells with negative and positive contrasts," *J. Biophotonics* **6**(5), 425–434 (2013).
28. K. V. Chakravarthy et al., "Doxorubicin-conjugated quantum dots to target alveolar macrophages and inflammation," *Nanomed.-Nanotechnol. Biol. Med.* **7**(1), 88–96 (2011).
29. J. Hong, D. Pei, and X. Guo, "Quantum dot-Eu^{3+} conjugate as a luminescence turn-on sensor for ultrasensitive detection of nucleoside triphosphates," *Talanta* **99**, 939–943 (2012).
30. M. J. Ruedas-Rama et al., "A chloride ion nanosensor for time-resolved fluorimetry and fluorescence lifetime imaging," *Anal.* **137**(6), 1500–1508 (2012).
31. G. Jiang et al., "Cascaded FRET in conjugated polymer/quantum dot/dye-labeled DNA complexes for DNA hybridization detection," *ACS Nano* **3**(12), 4127–4131 (2009).
32. W. R. Algar et al., "Quantum dots as simultaneous acceptors and donors in time-gated forster resonance energy transfer relays: characterization and biosensing," *J. Am. Chem. Soc.* **134**(3), 1876–1891 (2012).
33. J. C. Claussen et al., "Biophotonic logic devices based on quantum dots and temporally-staggered Forster energy transfer relays," *Nanoscale* **5**(24), 12156–12170 (2013).
34. P. J. Cywinski, A. J. Moro, and H.-G. Löhmannsröben, "Cyclic GMP recognition using ratiometric QD-fluorophore conjugate nanosensors," *Biosens. Bioelectron.* **52**, 288–292 (2014).
35. P. J. Cywinski et al., "Sensitive and selective fluorescence detection of guanosine nucleotides by nanoparticles conjugated with a naphthyridine receptor," *Anal. Bioanaly. Chem.* **399**(3), 1215–1222 (2011).
36. I. L. Medintz and N. Hildebrandt, Eds., *FRET - Förster Resonance Energy Transfer: From Theory to Applications*, 1st ed., Wiley-VCH Verlag GmbH & Co., Weinheim, Germany (2013).
37. J.-C. G. Buenzli, "Lanthanide luminescence for biomedical analyses and imaging," *Chem. Rev.* **110**(5), 2729–2755 (2010).
38. S. V. Eliseeva and J.-C. G. Buenzli, "Rare earths: jewels for functional materials of the future," *New J. Chem.* **35**(6), 1165–1176 (2011).
39. D. Geissler et al., "Six-color time-resolved forster resonance energy transfer for ultrasensitive multiplexed biosensing," *J. Am. Chem. Soc.* **135**(3), 1102–1109 (2013).
40. D. Geissler et al., "Quantum dot biosensors for ultrasensitive multiplexed diagnostics," *Angew. Chem. Int. Ed.* **49**(8), 1396–1401 (2010).
41. N. Hildebrandt, K. D. Wegner, and W. R. Algar, "Luminescent terbium complexes: superior Förster resonance energy transfer donors for flexible and sensitive multiplexed biosensing," *Coord. Chem. Rev.* **273–274**, 125–138 (2014).
42. D. Geißler et al., "Lanthanides and quantum dots as Förster resonance energy transfer agents for diagnostics and cellular imaging," *Inorg. Chem.* **53**, 1824–1838 (2014).
43. W. R. Algar et al., "Emerging non-traditional Förster resonance energy transfer configurations with semiconductor quantum dots: investigations and applications," *Coord. Chem. Rev.* 65–85 (2014).
44. N. Hildebrandt et al., "Quantum dots as efficient energy acceptors in a time-resolved fluoroimmunoassay," *Angew. Chem. Int. Ed.* **44**(46), 7612–7615 (2005).
45. L. J. Charbonniere et al., "Lanthanides to quantum dots resonance energy transfer in time-resolved fluoro-immunoassays and luminescence microscopy," *J. Am. Chem. Soc.* **128**(39), 12800–12809 (2006).
46. C.-A. J. Lin et al., "Design of an amphiphilic polymer for nanoparticle coating and functionalization," *Small* **4**(3), 334–341 (2008).
47. M. T. Fernandez-Argueelles et al., "Synthesis and characterization of polymer-coated quantum dots with integrated acceptor dyes as FRET-based nanoprobes," *Nano Lett.* **7**(9), 2613–2617 (2007).
48. F. Zhang et al., "Polymer-coated nanoparticles: a universal tool for biolabelling experiments," *Small* **7**(22), 3113–3127 (2011).
49. C. Geidel et al., "A general synthetic approach for obtaining cationic and anionic inorganic nanoparticles via encapsulation in amphiphilic copolymers," *Small* **7**(20), 2929–2934 (2011).
50. T. Nishioka et al., "New luminescent europium(III) chelates for DNA labeling," *Inorg. Chem.* **45**(10), 4088–4096 (2006).
51. T. Niebling et al., "Excitation dynamics in polymer-coated semiconductor quantum dots with integrated dye molecules: the role of reabsorption," *J. Appl. Phys.* **106**(10) (2009).

Piotr J. Cywiński studied physics at the Lodz University of Technology, Poland, and then he received his PhD degree from the same university. After 2 years as a Marie Curie postdoctoral researcher at the Friedrich-Schiller University Jena, he moved to the University of Potsdam to pursue research on quantum dots. Currently, he is a senior researcher in the nanopolyphotonics group at the Fraunhofer Institute for Applied Polymer Research.

Tommy Hammann studies chemistry at the University of Potsdam, Germany, and did his bachelor thesis in the group of Prof. H.-G. Löhmannsröben. Currently, he is a master's student at the same university and a research assistant at the Fraunhofer Institute for Applied Polymer Research.

Dominik Hühn studied physics at the Philipps-Universität Marburg, Germany, and did his diploma thesis in the group of Prof. W. J. Parak. Currently, he is a PhD student in the same work group. His research topic is the functionalization of nanoparticles toward biological applications.

Wolfgang Parak studied physics at the Technische Universität München, Germany, and then received his PhD degree from the Ludwig Maximilians Universität München, Germany. After two years as a postdoc in Berkely Wolfgang Parak, he became an assistant professor in München, Germany. Currently, he is full-time professor at the Philipps Universität Marburg. He is also associate editor of *ACS Nano*.

Niko Hildebrandt studied medical physics in Berlin and received a PhD degree in physical chemistry at the University of Potsdam in 2007. From 2008 to 2010, he was group leader at the Fraunhofer Institute for Applied Polymer Research. Since 2010 he has been a full-time professor at Université Paris-Sud, where he is leading the group of nanobiophotonics (www.nanofret.com) with a research focus on temporally and spectrally resolved Förster resonance energy transfer (FRET) spectroscopy and imaging for nanobiosensing.

Hans-Gerd Löhmannsröben studied physics at the Universities of Oldenburg, Göttingen and Chapel Hill. He received his PhD degree in Goettingen in 1985 and finished his Habilitation at the TU Braunschweig in 1994. After two professorships in Emden and Erlangen, he became chair professor of physical chemistry at Potsdam University in 2000. His research interests include photophysics and photochemisty, laser spectroscopy, and optical sensing. Since 2009 he has been a science ambassador for the state of Brandenburg.